

Structural basis of transcription inhibition by α -amanitin and implications for RNA polymerase II translocation

Florian Brueckner & Patrick Cramer

To study how RNA polymerase II translocates after nucleotide incorporation, we prepared elongation complex crystals in which pre- and post-translocation states interconvert. Crystal soaking with the inhibitor α -amanitin locked the elongation complex in a new state, which was refined at 3.4-Å resolution and identified as a possible translocation intermediate. The DNA base entering the active site occupies a 'pretemplating' position above the central bridge helix, which is shifted and occludes the templating position. A leucine residue in the trigger loop forms a wedge at the shifted bridge helix, but moves by 13 Å to close the active site during nucleotide incorporation. Our results support a Brownian ratchet mechanism that involves swinging of the trigger loop between open, wedged and closed positions, and suggest that α -amanitin impairs nucleotide incorporation and translocation by trapping the trigger loop and bridge helix.

The nucleotide addition cycle (NAC) of transcription begins with binding of a nucleoside triphosphate (NTP) substrate to the RNA polymerase (Pol) elongation complex (EC). The EC then incorporates a nucleotide into the growing RNA, generating a pyrophosphate ion and leading to the pretranslocation state. The polymerase subsequently translocates downstream along DNA and RNA to generate the post-translocation state and a free substrate binding site for the next NTP, completing the NAC. X-ray crystallography of Pol II ECs revealed how Pol II binds to DNA and RNA in the pretranslocation¹ and post-translocation states^{2,3}, and how it binds NTP in various ways²⁻⁴.

Despite this progress, the structural basis for translocation remains poorly understood. A comparison of the crystal structures of core Pol II and a bacterial RNA polymerase initially suggested that translocation involves a conformational change in the highly conserved bridge helix within the active center^{1,5}. The bridge helix stacked onto the end of the pretranslocation DNA-RNA hybrid, and its possible partial movement toward the hybrid was suggested to accompany nucleic acid movement during translocation^{1,5}. In a subsequent structure of another bacterial RNA polymerase, the central region of the bridge helix was flipped-out and contacted the adjacent, previously mobile trigger loop, which was suggested to influence bridge helix movement⁶. Biochemical studies of bacterial RNA polymerases revealed the functional cooperation of the bridge helix and trigger loop, and suggested more detailed models of translocation^{7,8}. Alternative bridge helix conformations were also observed within the same RNA polymerase, supporting the functional relevance of bridge helix movement^{9,10}.

The fungal toxin α -amanitin was suggested to interfere with bridge helix movement during translocation because it binds to the free Pol II core adjacent to the bridge helix¹¹. Kinetic data supported the idea that α -amanitin inhibits translocation¹². However, a difficulty with this model was that α -amanitin bound only one residue in the bridge helix, and this residue was separated by one turn from the residues that

apparently change conformation. An alternative model for inhibition suggested that α -amanitin interferes with movement of the trigger loop, which closes over the active site during nucleotide incorporation⁴.

To investigate structurally how Pol II translocation occurs, and how α -amanitin might interfere with it, we formed crystals of the complete Pol II EC in which the pre- and post-translocation states coexist. Soaking the inhibitor into such a crystal resulted in the structure of the α -amanitin-inhibited Pol II EC. This structure showed that α -amanitin traps the trigger loop in a new conformation and stabilizes the EC in a previously unobserved state that apparently corresponds to a translocation intermediate. The new structure leads to an extended model for the NAC and suggests how α -amanitin interferes with both nucleotide incorporation and Pol II translocation.

RESULTS

Coexistence of translocation states in EC crystals

Previous structures of the Pol II EC were not informative on the mechanism of translocation because they always revealed the same polymerase conformation, although the nucleic acids adopted either the pre- or the post-translocation conformation. As the EC is thought to exist in an equilibrium of pre- and post-translocation states in solution, we sought crystals of the complete Pol II EC that preserve this equilibrium. To detect the translocation state of nucleic acids within EC crystals, we labeled the DNA template strand in the hybrid with 5-bromouracil and determined the bromine position by anomalous diffraction. With the use of a minimal synthetic nucleic acid scaffold, two bromine peaks were observed, one peak at a height of 4.9 σ at position -4, indicating the post-translocation state, and one peak at a height of 7.9 σ at position -3, corresponding to the pretranslocation state (Fig. 1 and Methods; position +1 denotes the nucleotide incorporation site, and positive and negative numbers denote downstream and upstream positions, respectively). Thus, both translocation states coexisted within these crystals. As nucleic

Gene Center and Center for Integrated Protein Science Munich (CIPSM), Department of Chemistry and Biochemistry, Ludwig-Maximilians-Universität München, Feodor-Lynen-Strasse 25, 81377 Munich, Germany. Correspondence should be addressed to P.C. (cramer@LMB.uni-muenchen.de).

Received 9 May; accepted 5 June; published online 13 June 2008; doi:10.1038/nsmb.1458

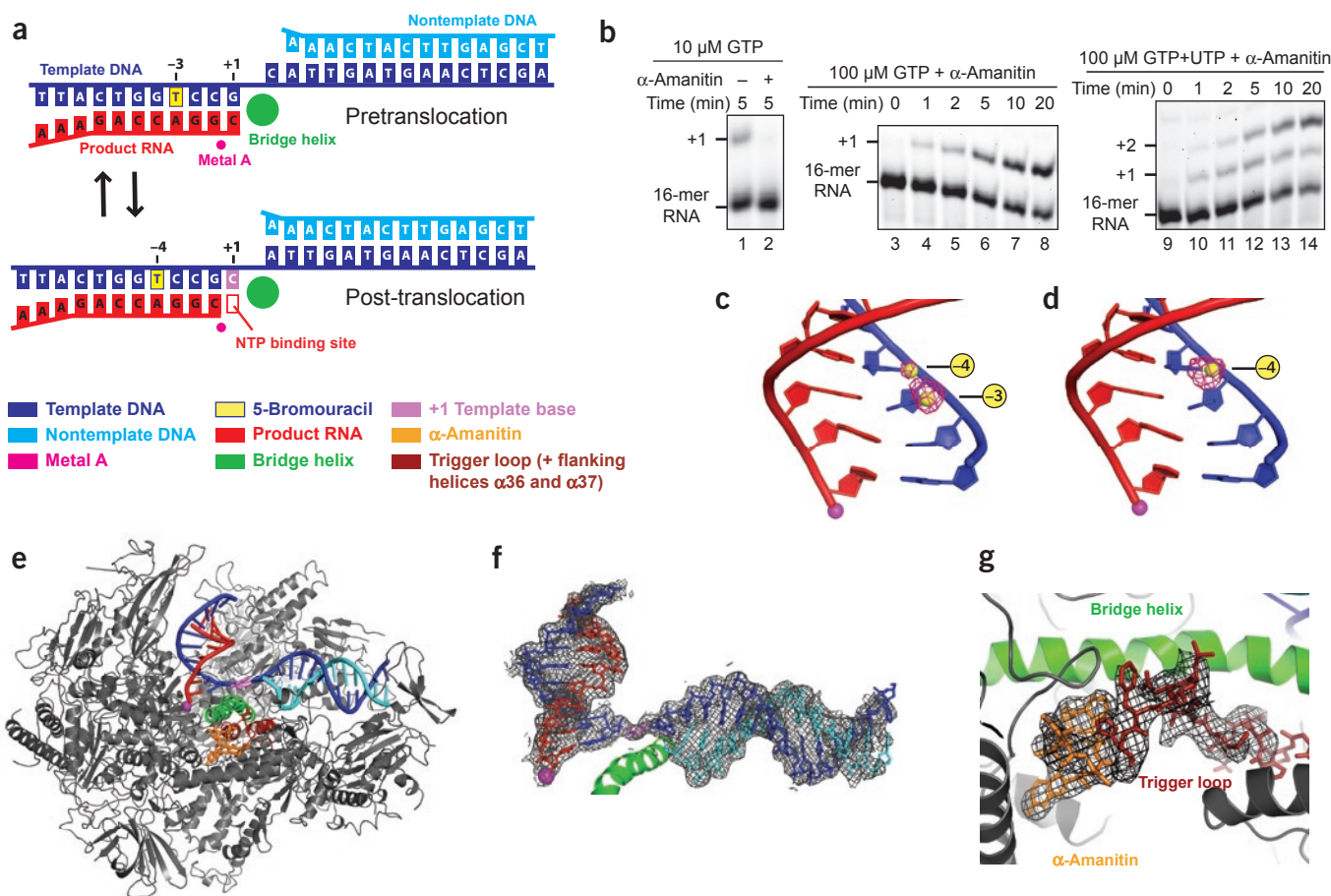


Figure 1 Structure of the α -amanitin-inhibited Pol II EC. **(a)** Pre- and post-translocation states. The nucleic acid scaffold used is depicted schematically with respect to the active-site metal ion A (magenta). The color key is used throughout. **(b)** Nucleotide incorporation and inhibition of the EC by α -amanitin. Inhibition of the EC was tested with a transcript extension assay (Methods). In the presence of α -amanitin and 10 μ M GTP, incorporation of the next complementary nucleotide was inhibited (lane 2). At higher substrate concentration (100 μ M), slow incorporation of one (lanes 3–8), or two (lanes 9–14) nucleotides is possible in the presence of α -amanitin. **(c, d)** Bromine anomalous difference Fourier maps (pink net) of the free EC **(c)** and the α -amanitin-inhibited EC **(d)**. The maps were calculated with phases from the Pol II model, after molecular replacement and rigid body refinement, and contoured at 4.4σ . The final model of the nucleic acids and metal A in the α -amanitin-inhibited EC is superimposed. In the absence of α -amanitin, two peaks were observed, coinciding with the locations of the bromine atom (yellow sphere) in a 5-bromouracil residue at positions -3 (4.9σ) and -4 (7.9σ) in the template strand (Methods). In the presence of α -amanitin, one peak was observed, coinciding with the location of the bromine atom (yellow sphere) in a 5-bromouracil residue at position -4 (7.8σ) in the template strand (Methods). The view is from the front⁹. **(e)** Overview of the α -amanitin-inhibited Pol II EC structure. The view is from the side². α -Amanitin (stick model), nucleic acids (base in pretemplating position as stick model), metal A, the bridge helix and the trigger loop (Leu1081 as stick model) are highlighted using the color key in **a**. Part of the protein is omitted for clarity. **(f)** Sigma-weighted $2F_o - F_c$ electron density map for the nucleic acids in the α -amanitin-inhibited EC. The map is calculated with phases from the refined model and contoured at 1.0σ . Nucleic acids, bridge helix and metal A of the refined model are superimposed. The view is as in **e**. **(g)** Unbiased initial $F_o - F_c$ electron density map for α -amanitin and the folded trigger loop. The map is calculated with phases from Pol II alone (Rpb1 residues 1076–1081 and 1092–1096 omitted) and contoured at 2.5σ . The refined model is superimposed, and helix $\alpha 37$ is omitted for clarity.

acids were not fixed by crystal contacts, we assumed that the two states interconvert in each EC of the crystal. The EC preparation used for crystallization was functional, as it supported RNA elongation, and was also sensitive to α -amanitin inhibition (Fig. 1b).

Structure of the α -amanitin-inhibited EC

To investigate the influence of α -amanitin on the apparent translocation equilibrium, we soaked the inhibitor into an EC crystal and solved the structure by molecular replacement with the Pol II structure (Fig. 1e and Methods). We achieved a resolution of 3.4 Å, which reveals even subtle conformational changes and represents an advance over the best previously obtained resolution for a complete Pol II EC (3.8 Å; Methods). We observed only a single bromine peak at a height of 7.8σ that unambiguously revealed the post-translocation register of the hybrid (Fig. 1d). Strong unbiased difference electron density was present for

the hybrid, for the entire downstream DNA, for α -amanitin and for the N-terminal region of the previously disordered trigger loop (Fig. 1f,g).

The structure was rebuilt and carefully refined (Methods), and revealed that α -amanitin occupies the site observed in the free Pol II core-amanitin complex¹¹ but shows an altered set of contacts with Pol II (Fig. 2 and Table 1). In particular, the inhibitor formed two previously unobserved hydrogen bonds with the Rpb1 residue His1085 within the N-terminal part of the trigger loop (Fig. 2). Because the trigger loop is disordered in the free EC, α -amanitin restricts trigger loop movement. In addition to the previously observed contact of α -amanitin to the bridge helix residue Glu822 (ref. 11), several indirect contacts to the bridge helix were observed. In particular, α -amanitin contacts residues Gln767, Gln768, Ser769 and Gly772 in the Rpb1 loop $\alpha 23$ - $\alpha 24$, which in turn binds the bridge helix residues His816 and Glu822 with its residues Gln768 and Glu771, respectively (Fig. 2 and

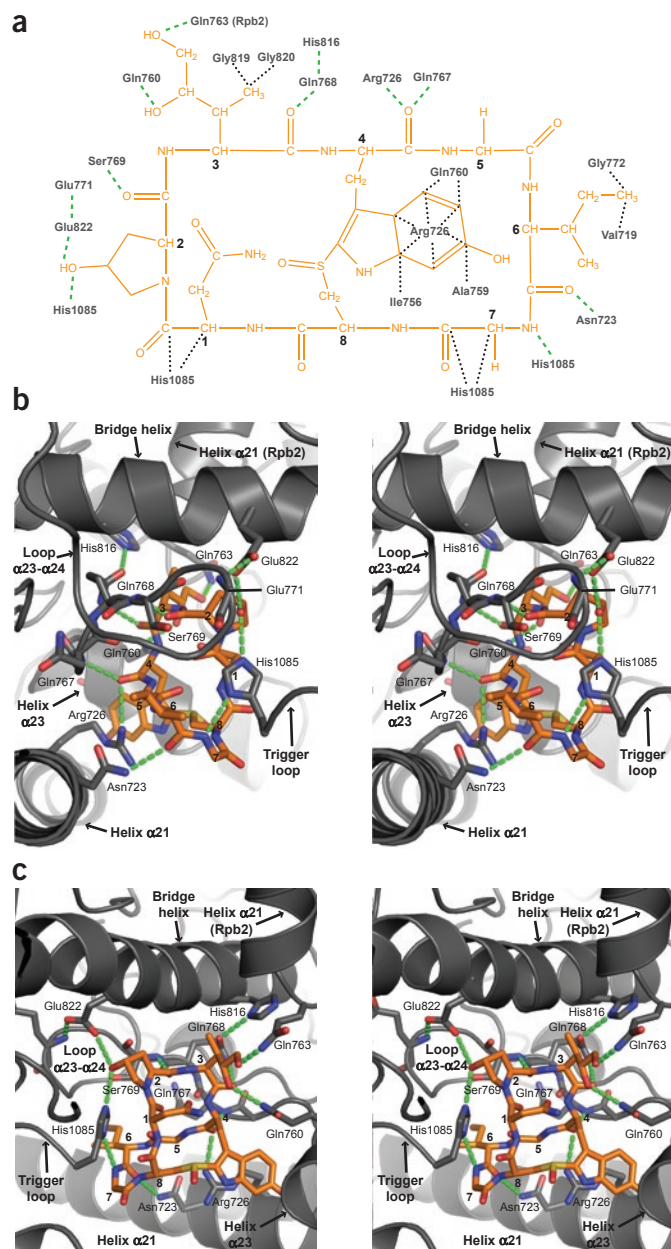


Figure 2 Contacts between α -amanitin and Pol II. (a) Schematic representation of Pol II– α -amanitin contacts. The chemical formula of α -amanitin is shown in orange. Pol II residues in contact with the inhibitor are depicted in gray. All residues are from Rpb1 except for Gln763, which belongs to Rpb2. Hydrogen bonds are depicted as green dashed lines, and hydrophobic contacts as black dotted lines. Numbers of α -amanitin residues are shown next to their $C\alpha$ atoms³⁰. (b, c) Stereoviews of α -amanitin in its binding pocket. α -Amanitin is depicted as a stick model with carbon atoms in orange. Pol II is shown as a ribbon model in gray, with selected residues of the binding pocket shown in stick model with carbon atoms in gray. Nitrogen, oxygen and sulfur atoms are blue, red and yellow, respectively. Hydrogen bonds are depicted as green dashed lines. Numbers of α -amanitin residues are shown next to their $C\alpha$ atoms. Pol II elements and residues that contribute to the binding pocket are labeled and belong to Rpb1, except for helix α 21 and Gln763, which belong to Rpb2. The two views depicted are related by an $\sim 120^\circ$ rotation around a vertical axis. In **b**, the view is from the front, similar to **Figure 1g**, and in **c** the view is from the back.

a wedge between Val829 in the bridge helix and Pro1099 in helix α 37 (helix G' in bacterial RNA polymerase; **Fig. 3b–d**). These observations are consistent with a concerted movement of the central bridge helix and the trigger loop during translocation.

New state of the EC as a translocation intermediate

The shifted central bridge helix and wedged trigger loop stabilize the nucleic acids in a previously unobserved conformational intermediary between the pre- and post-translocation conformations. Whereas the hybrid adopts the post-translocation position (**Figs. 1d** and **3e, g**), the downstream DNA template adopts an intermediary position that corresponds to incomplete translocation (**Fig. 3e–g**). The incoming DNA template base at register +1 adopts a previously unobserved position above the central bridge helix (in the side and front views, **Fig. 3d–g**). We refer to this new template base position as the 'pretemplating' position. In the free EC, the +1 base occupies a standard 'templating' position opposite the NTP binding site. In the templating position, the +1 base is twisted by 90° with respect to the +2 base and stacks against residues Ala832 and Thr831 in the central bridge helix (**Fig. 4**). In the new structure, the templating site is occluded by the shifted central bridge helix, in particular by the Ala832 side chain (**Figs. 4c, d**). A previously observed conformational change in the bridge helix did not include residues Thr831 and Ala832 (ref. 4; **Fig. 4g**) and is unlikely to be relevant for translocation. In the new EC state, the +1 base is not twisted with respect to the +2 base and retains contacts with the +2 base downstream, although the base stacking is discontinued (**Fig. 3f**). These considerations suggest that the state of the Pol II EC that is induced by α -amanitin binding to interconverting pre- and post-translocation ECs is a translocation intermediate. The EC is apparently trapped after translocation of the hybrid to the post-translocation position, but before complete delivery of the +1 base to the templating position in the active site (opposite the NTP binding site), and thus before full establishment of the post-translocation state.

DISCUSSION

Here we report the structure of the Pol II EC in a new, α -amanitin-inhibited state, which is intermediary between the pre- and post-translocation states. In this structure, the DNA–RNA hybrid adopts the post-translocation position, and the downstream DNA template adopts a new position between the pre- and post-translocation register. The +1 base in the template strand occupies a previously unobserved pretemplating site above the bridge helix. The central bridge helix is shifted upstream and partially occludes the templating site that is occupied by the +1 base in

Table 1). The hydroxyl group of the hydroxyproline residue of α -amanitin is also near the Rpb1 residue Asn1082 of the trigger loop, which in turn binds Asp826 in the bridge helix. Thus, an intricate network of hydrogen bonds and other contacts exists between α -amanitin, the trigger loop, the bridge helix and Rpb1 loop α 23– α 24.

The trigger loop forms a wedge at the bridge helix

The refined structure showed that binding of α -amanitin locked the Pol II EC into a defined, previously unobserved conformational state. The bridge helix remained helical along its entire length, but its central part (two turns, residues Asp826 to Glu833, termed here the central bridge helix) was shifted upstream in the direction of the hybrid, as observed in the unbiased difference Fourier map (**Fig. 3**). The side chain of Rpb1 residue Ala832 moved by 2.5 \AA in the direction of DNA template translocation. The trigger loop apparently stabilizes the shifted conformation of the central bridge helix, as its residue Leu1081 forms

Table 1 Hydrogen bonds between α -amanitin and Pol II residues

α -Amanitin residue	α -Amanitin atom ^a	Pol II residue ^b	Pol II atom ^a	Length (Å)	Present in core Pol II– α -amanitin complex ¹¹
2	OD (A)	His1085 (TL)	NE2 (D)	2.9	no
2	OD (D)	Glu822 (BH)	OE1 (A)	3.1	yes
2	O (A)	Ser769	N (D)	3.1	yes
3	OD (A)	Gln763 (Rpb2)	NE2 (D)	2.5	no
3	OG (A)	Gln760	NE (D)	3.0	no
3	O (A)	Gln768	NE2 (D)	3.4	yes
4	O (A)	Arg726	NH1 (D)	3.2	yes
4	O (A)	Gln767	N (D)	2.8	yes
6	O (A)	Asn723	ND2 (D)	3.2	no
7	N (D)	His1085 (TL)	ND1 (A)	3.0	no

^aA, acceptor; D, donor. ^bBH, bridge helix; TL, trigger loop.

the pre- and post-translocation states. The trigger loop is in a position to form a wedge that stabilizes the shifted bridge helix.

Combining the new structure with known EC structures of Pol II^{1,2,4} and a bacterial RNA polymerase¹³ leads to a model of the NAC (Fig. 5) that extends previous models^{1,7,8,13–15}. In this model, NTP binds to the post-translocation EC in a preinsertion state that maintains an open, flexible trigger loop^{2,13}. Subsequent movement of the NTP to the

insertion site goes along with closure of the trigger loop and formation of the catalytically active polymerase conformation^{4,13}. Catalytic incorporation of the nucleotide into the RNA leads to pyrophosphate formation. Release of pyrophosphate could then enable movement of the trigger loop to the wedged position, facilitating a shift in the central bridge helix, which accompanies movement of the nucleic acids to the intermediary state (translocation step 1). Release of the wedge and relaxation of the bridge helix to the straight position frees the templating site for the next incoming template base and thereby enables movement of the nucleic acids to the post-translocation state, which completes the NAC (translocation step 2).

Our data suggest a two-step mechanism of nucleic acid translocation via an intermediate (compare Figs. 3e–g and 5). During step 1, the hybrid moves from the pre- to the post-translocation position, and the downstream DNA translocates until the next DNA template base (register +2) reaches the pretemplating site. During step 2, the DNA base twists by 90° to reach its templating position in the active center (register +1). This twisting is accompanied by a flipping of the phosphate backbone group between

Figure 3 The α -amanitin-inhibited EC structure is apparently a translocation intermediate. **(a)** The shifted central bridge helix. The $F_o - F_c$ electron density omit map contoured at 2.5σ is shown in blue. The map was calculated with phases from the final model lacking the bridge helix (Rpb1 residues 810–845). The unbiased $F_o - F_c$ difference map, calculated with initial phases from the Pol II model, is contoured at 2.5σ and shown in red. The final model of the bridge helix is superimposed, and residues Ala832 and Thr831 are highlighted in yellow and brown, respectively. **(b,c)** The trigger loop forms a wedge between the bridge helix and helix $\alpha 37$. Top views⁵ of a ribbon model in **b** and a space-filling model in **c** are shown. The wedging trigger loop residue Leu1081 and the residues flanking it (Val829 and Pro1099) are shown in lighter colors. **(d)** The +1 DNA template base adopts a pretemplating position. The initial unbiased $F_o - F_c$ difference map for the nucleic acids is shown around the +1 position, contoured at 2.5σ . The +1 base in the pretemplating site is highlighted in violet. The view is from the top. **(e–g)** Transition from the apparent translocation intermediate to the post-translocation state. The structures of the α -amanitin inhibited Pol II EC (apparent translocation intermediate) and the post-translocation EC (ref. 2) were superimposed. Metal A, nucleic acids, the bridge helix and the trigger loop including its flanking helices $\alpha 36$ and $\alpha 37$ are shown. The elements of the post-translocation EC structure are depicted in lighter colors. The bridge helix is shown as a C_α trace. In **e** and **g**, phosphates and bases are depicted as balls and sticks, respectively. Conformational transitions during translocation step 2 that are required to convert the intermediate to the post-translocation EC are indicated with arrows and numbered 1–5. The view is from the side **(e)**, as in **Figure 1e**, or from the top **(f,g)**, as in **Figure 3b**.

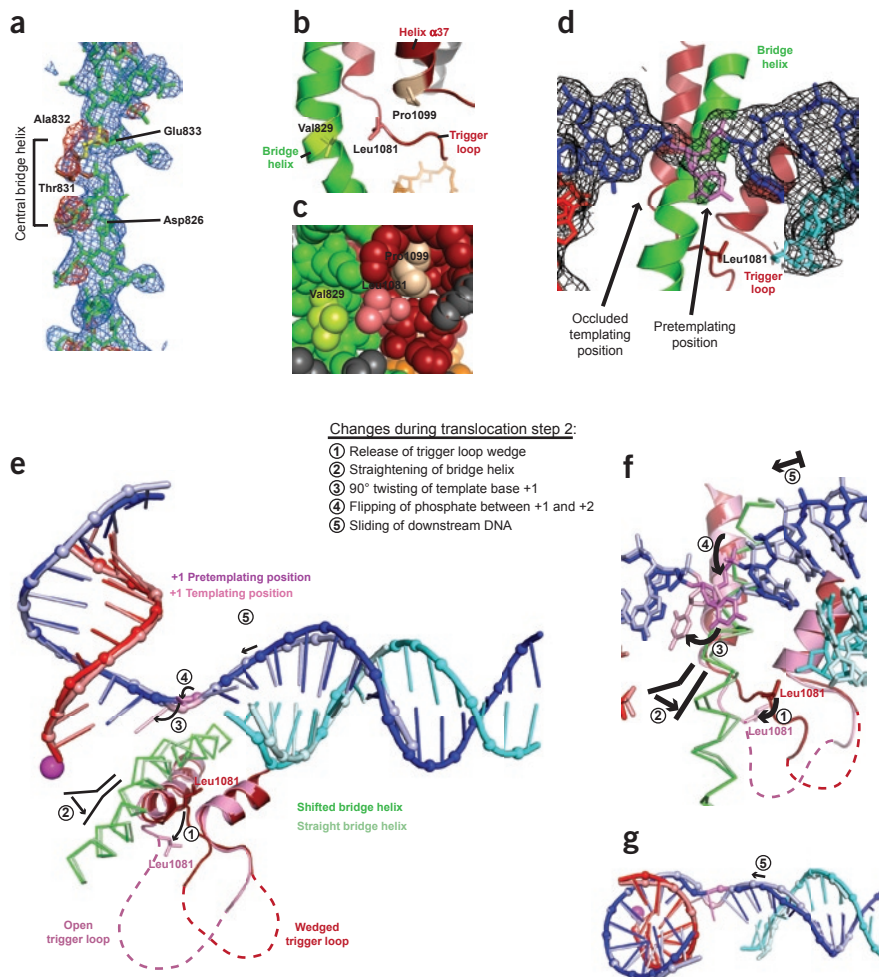
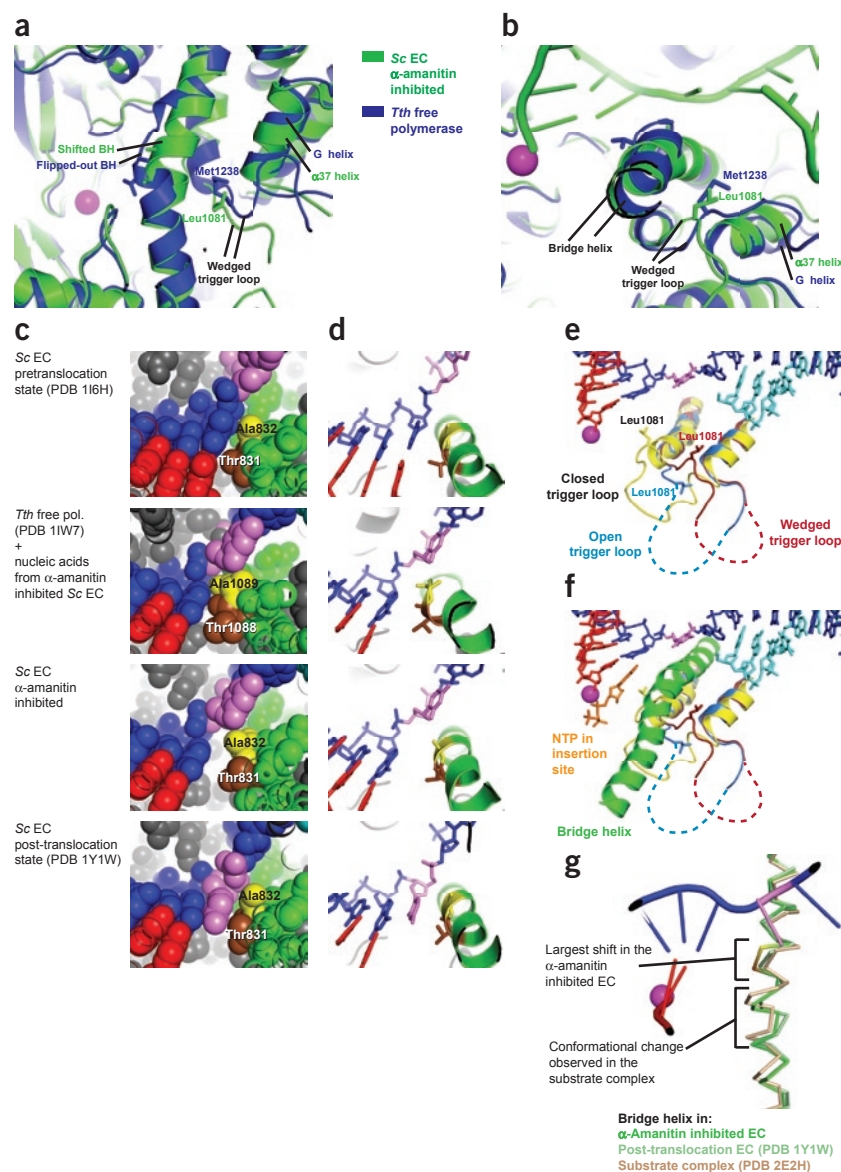


Figure 4 Comparisons with bacterial RNA polymerase and possible EC states. (a,b) Superposition of the trigger loops and bridge helices in the α -amanitin inhibited Pol II EC and the free *T. thermophilus* (*Tth*) RNA polymerase⁶. The trigger loop residue Leu1081 (*S. cerevisiae* (*Sc*) Pol II) or its homologous residue Met1238 (*Tth*) forms a wedge between the bridge helix and helix α 37 in Pol II or G' in *Tth*. The views are from the top (a) or the side (b), as in **Figure 3b** or **1e**, respectively. In the α -amanitin-inhibited Pol II EC, the central bridge helix is shifted, whereas in the bacterial holoenzyme it adopts a flipped-out conformation. (c,d) Four possible states of the EC. Above to below, the pretranslocation state (PDB 1I6H)¹, a potential transition state with a modeled flipped-out bridge helix (PDB 1IW7)¹⁷, the α -amanitin-inhibited EC (the apparent translocation intermediate with the shifted bridge helix, this study), and the post-translocation state (PDB 1Y1W)² are shown with space-filling models (c) or ribbon diagrams (d). The bridge helix residues Ala832/Ala1089 (Pol II/*Tth*) and Thr831/Thr1088 (Pol II/*Tth*) are highlighted in yellow and brown, respectively. (e,f) Comparison of trigger loop conformations. Pol II EC structures in the post-translocation state (PDB 1Y1W)², with bound NTP substrate (PDB 2E2H)⁴, and in the intermediary state are superimposed. Nucleic acids and metal A are from the translocation intermediate. The trigger loops of the three structures are depicted in dark red (wedged, translocation intermediate), light blue (open, 1Y1W) and yellow (closed, 2E2H, labels in black). (f) Also depicted are the bridge helix (green, apparent translocation intermediate) and the NTP in the insertion site (orange, 2E2H). (g) Comparison of bridge helix conformations in the α -amanitin-inhibited EC (green, with residues Ala832 and Thr831 highlighted in yellow and brown, respectively), the post-translocation EC² (light green) and the core Pol II EC with bound NTP⁴ (beige).



the DNA template bases +1 and +2, and a sliding of the downstream DNA to the post-translocation position. In the potential intermediate, many contacts between the polymerase and the nucleic acids are maintained. This probably preserves EC stability during translocation and decreases the energy barrier between pre- and post-translocation states.

The EC acts like a helicase on the incoming DNA duplex that apparently melts the base pair +2 downstream of the active site^{16,17}. Modeling shows that the DNA base in the pretemplating position of the intermediate cannot remain base-paired with its counterpart in the nontemplate strand, because the path of the template strand strongly deviates from the course of canonical B-DNA, as suggested², and the path of the nontemplate strand is blocked by fork loop 2 (refs. 1,2,4,18). Available data thus suggest that RNA polymerase melts the downstream DNA base pair during translocation step 1.

Previous structural and biochemical data for bacterial RNA polymerases suggest the existence of a translocation intermediate and support our findings and interpretations. In the structures of the free *Thermus thermophilus* RNA polymerase holoenzyme⁶ and the *Thermus aquaticus* RNA polymerase (referred to hereafter as *Tth* and *Taq*, respectively) bound to two different antibiotics¹⁹, the trigger loop

residue Met1238 intrudes between the bridge helix and helix G' (α 37 in Pol II), similarly to the corresponding Pol II trigger loop residue Leu1081, which forms a wedge in the apparent intermediate (Figs. 3b,c and 4a,b). In these bacterial polymerase structures, the central bridge helix adopts a flipped-out conformation in the region that is shifted in the Pol II EC intermediate (*Tth* and *Taq* residues 1087–1092).

RNA-protein cross-linking suggested that the flipped-out conformation reflects an intermediary state between the pre- and post-translocation states, and that the bridge helix and trigger loop undergo a cooperative structural transition during nucleotide incorporation and translocation⁸. Furthermore, cross-linking studies with *Escherichia coli* RNA polymerases carrying mutations in the C-terminal part of the trigger loop suggested a role of the trigger loop in controlling bridge helix movement⁷. Finally, mutation of residue Met932 in *E. coli* RNA polymerase, which corresponds to the wedged trigger loop residue Leu1081 in Pol II, strongly increases the duration of transcriptional pausing²⁰, consistent with an important role of this residue not only in nucleotide incorporation but also in translocation.

These published data and our results converge on a conserved translocation mechanism for all multisubunit RNA polymerases,

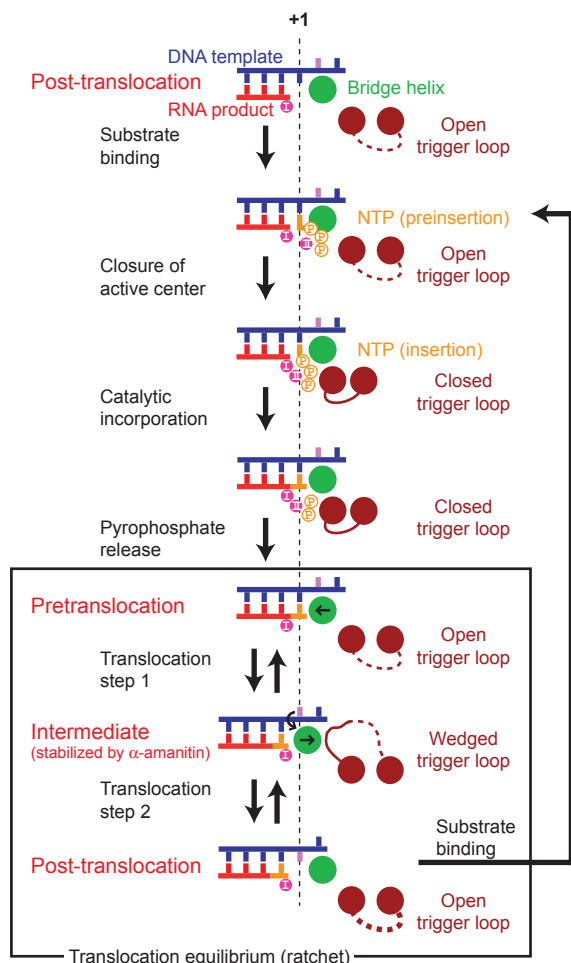


Figure 5 Model of the nucleotide addition cycle (NAC). Schematic representation of the extended model for the NAC. The vertical dashed line indicates register +1. For details, refer to text.

involving a trigger loop–stabilized EC intermediate with an altered structure of the central bridge helix. Owing to the high conservation of the active center in all multisubunit RNA polymerases, the observed Pol II EC intermediate conformation is likely to exist in the bacterial EC, although this remains to be shown, because the central bridge helix is straight in the first bacterial EC structure¹⁷. Whether the flipped-out conformation of the bridge helix can be adopted within an EC also remains to be demonstrated by structural analysis. Modeling shows that the flipped-out bridge helix can be accommodated within the Pol II EC intermediate structure (Fig. 4c,d). In this model, the *Tth* bridge helix residues Thr1088 and Ala1089 (Thr831 and Ala832 in Pol II) stack against the –1 base of the DNA template strand (Fig. 4c,d). This EC conformation, if it exists, could represent the transition state of translocation step 1 (in case the central bridge helix is transiently flipped out and this state does not represent a local energy minimum).

Whereas our studies provide insights into the structural transitions of the EC during translocation, a Brownian ratchet model may explain the directionality of translocation^{7,15,21}. The model assumes that the ground state of the EC is characterized by an equilibrium between rapidly interconverting pre- and post-translocation states (the ratchet), enabled by an oscillation between different bridge helix conformations. NTP binding temporarily stops the oscillation, acting like a pawl of

a ratchet. After nucleotide incorporation, oscillation resumes around the next template position. In this model, the energy for translocation comes from Brownian fluctuations, and the directionality of translocation results from trapping the forward fluctuation by NTP binding and nucleotide incorporation.

Our data support the Brownian ratchet mechanism. First, the proposed equilibrium between pre- and post-translocation states is apparently observed within crystals as coexisting, interconverting states of the EC. Second, the interruption of bridge helix oscillation by NTP binding may be rationalized by the mutually exclusive functions of the trigger loop during bridge helix shifting and NTP incorporation. The trigger loop residue Leu1081 (Met1238 in *Tth* and *Taq*) forms a wedge at the shifted bridge helix in the intermediate (Figs. 3b,c and 4a,b), but moves by up to 13 Å to close over the NTP during nucleotide incorporation^{4,13}. Thus, swinging of the trigger loop between closed and wedged positions is apparently important for the NAC and the Brownian ratchet.

Trigger loop swinging may also be important for transcription fidelity. We have previously shown that an abasic site at template position +1 causes nontemplated nucleotide incorporation²². This could also occur in the intermediate, which lacks a base in the templating position but provides enough space to bind the NTP. However, nucleotide incorporation is not favored in the intermediate, because the trigger loop adopts the wedged position and is not available for active-site closure.

The mechanism of substrate incorporation and translocation was well studied for the single-subunit RNA polymerase from bacteriophage T7 (refs. 23,24). This polymerase shares no sequence similarity with the multisubunit enzymes, but the arrangement of nucleic acids and many mechanistic aspects are similar^{15,17,25}. Structures for the T7 EC include a product complex, which contained the nucleic acids in the pretranslocation state after nucleotide incorporation and retained the pyrophosphate²⁴. In this structure, the so-called O-helix binds the DNA template strand and the pyrophosphate with its C- and N-terminal ends, respectively. Pyrophosphate release apparently triggers a 22° rotation of the O-helix that results in translocation²⁴. This observation suggested that the catalytic event induces a conformational change that actively drives translocation in a power-stroke mechanism, an alternative to the Brownian ratchet.

In T7 RNA polymerase, a single structural element, the O-helix, is involved in both pyrophosphate binding and template translocation, whereas Pol II uses two elements for these functions, the trigger loop and the bridge helix. A product-complex structure is not available for Pol II, but the pyrophosphate may retain the trigger loop in a closed position, such that only its release remobilizes the trigger loop, which could then adopt the wedged position and re-establish the translocation equilibrium of a ratchet. Because the trigger loop passes through a mobile state between the closed and wedged positions, it cannot induce a power stroke by directly shifting the bridge helix. Instead, the trigger loop wedge stabilizes a conformational state of the bridge helix that accompanies and facilitates nucleic acid translocation. Single-molecule studies are consistent with a Brownian ratchet^{26,27}.

Our data suggest that α -amanitin inhibits Pol II by trapping the wedged trigger loop and shifted bridge helix, thereby stabilizing a conformation of the EC that apparently represents a translocation intermediate. This model predicts that α -amanitin interferes with both nucleotide incorporation and translocation, consistent with published functional data. α -Amanitin strongly reduces the polymerase elongation rate but does not influence its NTP affinity and does not abolish the addition of multiple nucleotides^{28,29}. Our elongation assays provided consistent results (Fig. 1b). Kinetic studies distinguished three EC conformations with different sensitivities for α -amanitin¹². It seems that these EC conformations, which showed high, medium or no sensitivity to α -amanitin inhibition¹², correspond to the intermediate, the pre- and the post-translocation state, respectively.

Table 2 Data collection and refinement statistics

	Complete Pol II EC with coexisting pre- and post- translocation states	α -Amanitin-inhibited complete Pol II EC
Data collection		
Space group	C222 ₁	C222 ₁
Cell dimensions		
<i>a</i> , <i>b</i> , <i>c</i> (Å)	221.9, 393.1, 283.3	220.6, 394.2, 284.0
Resolution (Å)	50–3.60 (3.73–3.60)*	50–3.40 (3.52–3.40)
<i>R</i> _{sym} (%)	6.7 (36.8)	13.3 (46.7)
<i>I</i> / σ <i>I</i>	15.9 (3.9)	8.5 (3.0)
Completeness (%)	99.9 (99.9)	99.9 (99.9)
Redundancy	3.8 (3.6)	3.6 (3.5)
Refinement		
Resolution (Å)		50–3.40
No. reflections		328,642
<i>R</i> _{work} / <i>R</i> _{free}		25.5 / 28.8
No. atoms		
Protein		31,025
Ions		9
Nucleic acids		985
α -Amanitin		64
<i>B</i> -factors		
Protein		97.3
Ions		81.2
Nucleic acids		160.9
α -Amanitin		90.3
R.m.s. deviations		
Bond lengths (Å)		0.009
Bond angles (°)		1.5

*Values in parentheses are for highest-resolution shell.

A network of direct and indirect contacts between α -amanitin, the bridge helix and the trigger loop apparently underlies polymerase inhibition. Analysis of amanitin derivatives showed that the hydroxyl group of the hydroxyproline residue 2 of α -amanitin is crucial for inhibition^{30,31}. The importance of this hydroxyl group can now be ascribed not only to its contact to the bridge helix residue Glu822 (ref. 11), but also to its interaction with the trigger loop residue His1085 and a possible contact to Asn1082, which binds the bridge helix residue Glu826 (Fig. 2). Because α -amanitin stays attached to the active EC²⁹, some of its contacts with Pol II, in particular with the trigger loop and bridge helix, apparently get broken during the NAC. The energy required to break these contacts may be responsible for the strong reduction in the elongation rate in the presence of the toxin. In particular, the incoming NTP may induce a shift of the template base from the pretemplating to the templating position, resulting in the unproductive preinsertion substrate state observed for the bacterial EC inhibited by streptolydigin¹⁴. The inhibitory mechanisms of streptolydigin and α -amanitin may thus be similar; both compounds bind to adjacent sites of the EC and contact the trigger loop and bridge helix.

METHODS

Preparation of Pol II ECs. Endogenous *Saccharomyces cerevisiae* ten-subunit Pol II core enzyme and recombinant Rpb4–Rpb7 heterodimer were purified as described^{32,33}. Nucleic acid scaffolds (Fig. 1a) were annealed by mixing equimolar

amounts of synthetic template DNA, nontemplate DNA and RNA in Tris buffer, pH 7.4, at a final concentration of 100 μ M, heating the mixture to 95 °C for 5 min and slow-cooling to 4 °C in a thermocycler. Stoichiometric Pol II ECs were assembled by incubating core Pol II for 10 min with 2 molar equivalents of nucleic acid scaffold, followed by 20 min incubation with 5 molar equivalents of recombinant Rpb4–Rpb7 in 50 mM HEPES, pH 7.5, 40 mM ammonium sulfate, 10 μ M ZnCl₂, 5% (v/v) glycerol, 10 mM DTT at 20 °C. The complexes were purified by size-exclusion chromatography (Superose 6 10/300 GL, GE Healthcare) in 5 mM HEPES, pH 7.25, 40 mM ammonium sulfate, 10 μ M ZnCl₂ and 10 mM DTT.

Crystallization and crystal treatment. Purified Pol II ECs were concentrated to 3.5–4.5 mg ml⁻¹ and extra nucleic acid scaffold was added before crystallization to a final concentration of 2 μ M. Crystals were grown at 22 °C with the hanging-drop vapor diffusion method by mixing 2 μ l of sample solution with 1 μ l of reservoir solution (200 mM ammonium acetate, 300 mM sodium acetate, 50 mM HEPES, pH 7.0, 4–7% (w/v) PEG 6000 and 5 mM Tris(2-carboxyethyl) phosphine (TCEP)). Crystals were harvested in mother solution after 10–20 d, when they had reached their maximum size (approximately 0.4 \times 0.3 \times 0.2 mm). We transferred the crystals stepwise over 5 h to mother solution containing additionally 0–22% (v/v) glycerol. For complex formation with α -amanitin (Sigma), the crystals were incubated for 4 h in mother solution containing additionally 22% (v/v) glycerol, 5 mM magnesium acetate and 100 μ M α -amanitin. Crystals were slowly cooled to 8 °C and flash-cooled by plunging into liquid nitrogen.

X-ray structure analysis. Diffraction data were collected in 0.25° increments at the protein crystallography beamline X06SA of the Swiss Light Source using the new Pilatus 6M pixel detector³⁴ and a wavelength of 0.91908 Å (Table 2). Raw data were processed with XDS³⁵. Structures were solved by molecular replacement with the program Phaser³⁶, using the structure of the complete 12-subunit Pol II EC without nucleic acids as a search model (PDB 1Y1W)². The molecular replacement solution was subjected to rigid body refinement with CNS version 1.2 (ref. 37) using five rigid groups (core, jaw-lobe, shelf, clamp and Rpb4–Rpb7). We built the model using programs Coot³⁸, O³⁹, and Moloc⁴⁰. The nucleic acids were built into the initial *F*_o–*F*_c electron density map. The register of the nucleic acids was unambiguously defined by bromine labeling as described³³. Shifted parts of the trigger loop and the bridge helix were manually rebuilt into omit maps (Figs. 1g and 3a). A model for α -amanitin¹¹ was manually placed into the initial *F*_o–*F*_c map (Fig. 1g) and adjusted manually and by restrained real-space refinement with Moloc. Atomic positions and B-factors were refined with CNS version 1.2. Refinement parameters for α -amanitin were generated using Moloc. Refinement was monitored with the free *R* factor, calculated from the same 2% set of excluded reflections as in refinement of complete Pol II⁴¹ and the complete Pol II EC², extended to the higher resolution of 3.4 Å. The increase in resolution was apparently due to differences in the crystallization protocol, use of a new, highly sensitive pixel detector with increased signal-to-noise ratio and an improved processing strategy, including the use of XSCALE with zero-dose extrapolation for scaling and CNS version 1.2 with bulk solvent parameter grid search for refinement and map calculation. In the refined structure, 98.4% of the residues fall in allowed regions of the Ramachandran plot (calculated with Procheck version 3.5 (ref. 42)). Structural superposition was performed with the secondary-structure matching function of Coot³⁸. Figures were prepared with PyMOL (<http://pymol.sourceforge.net>).

Transcript extension assays. Stoichiometric ECs of complete Pol II, containing the ten-subunit core and Rpb4–Rpb7 were assembled and purified as described above, but in transcription buffer (20 mM HEPES, pH 7.6, 60 mM ammonium sulfate, 10 μ M ZnCl₂, 10% (v/v) glycerol and 10 mM DTT). α -Amanitin-inhibited Pol II ECs were prepared by incubating ECs at 20 °C with α -amanitin for 10 min. The RNAs used for extension assays were identical to those used for structural studies, except for five additional nucleotides (5'-UGCAU-3') and a fluorescein label at their 5' end. For transcript extension, ECs or α -amanitin-inhibited ECs were incubated with NTPs and 10 mM magnesium sulfate at 28 °C in transcription buffer. Reactions were stopped by incubating with an equal volume of gel loading buffer (90% (v/v) formamide, 50 mM EDTA, pH 7.4) for 5 min at 95 °C. The RNA products were separated by denaturing gel electrophoresis (0.5 pmol RNA per lane, 0.4 mm 20% (w/v) polyacrylamide gels containing 7 M urea, 50–55 °C) and visualized with a Typhoon 9400 scanner (GE Healthcare).

Accession code. Protein Data Bank: Coordinates and structure factors of the complete Pol II EC- α -amanitin complex crystal structure have been deposited under accession code 2VUM.

ACKNOWLEDGMENTS

We thank D. Kostrewa and other members of the Cramer laboratory for help. We thank D. Temiakov for discussions. E.B. was supported by the Nanosystems Initiative Munich (NIM) and the Elitenetzwerk Bayern (ENB). P.C. was supported by the Deutsche Forschungsgemeinschaft, the Sonderforschungsbereich SFB646, the Transregio 5 Chromatin, the EU research grant network 3D Repertoire and the Fonds der Chemischen Industrie. Part of this work was performed at the Swiss Light Source (SLS) at the Paul Scherrer Institut, Villigen, Switzerland.

Published online at <http://www.nature.com/nsmb/>

Reprints and permissions information is available online at <http://npg.nature.com/reprintsandpermissions/>

- Gnatt, A.L., Cramer, P., Fu, J., Bushnell, D.A. & Kornberg, R.D. Structural basis of transcription: an RNA polymerase II elongation complex at 3.3 Å resolution. *Science* **292**, 1876–1882 (2001).
- Kettenberger, H., Armache, K.-J. & Cramer, P. Complete RNA polymerase II elongation complex structure and its interactions with NTP and TFIIS. *Mol. Cell* **16**, 955–965 (2004).
- Westover, K.D., Bushnell, D.A. & Kornberg, R.D. Structural basis of transcription: nucleotide selection by rotation in the RNA polymerase II active center. *Cell* **119**, 481–489 (2004).
- Wang, D., Bushnell, D.A., Westover, K.D., Kaplan, C.D. & Kornberg, R.D. Structural basis of transcription: role of the trigger loop in substrate specificity and catalysis. *Cell* **127**, 941–954 (2006).
- Cramer, P., Bushnell, D.A. & Kornberg, R.D. Structural basis of transcription: RNA polymerase II at 2.8 Å resolution. *Science* **292**, 1863–1876 (2001).
- Vassilyev, D.G. *et al.* Crystal structure of a bacterial RNA polymerase holoenzyme at 2.6 Å resolution. *Nature* **417**, 712–719 (2002).
- Bar-Nahum, G. *et al.* A ratchet mechanism of transcription elongation and its control. *Cell* **120**, 183–193 (2005).
- Epshtein, V. *et al.* Swing-gate model of nucleotide entry into the RNA polymerase active center. *Mol. Cell* **10**, 623–634 (2002).
- Tuske, S. *et al.* Inhibition of bacterial RNA polymerase by streptolydigin: stabilization of a straight-bridge-helix active-center conformation. *Cell* **122**, 541–552 (2005).
- Artsimovitch, I. *et al.* Allosteric modulation of the RNA polymerase catalytic reaction is an essential component of transcription control by rifamycins. *Cell* **122**, 351–363 (2005).
- Bushnell, D.A., Cramer, P. & Kornberg, R.D. Structural basis of transcription: α -amanitin-RNA polymerase II cocrystal at 2.8 Å resolution. *Proc. Natl. Acad. Sci. USA* **99**, 1218–1222 (2002).
- Gong, X.Q., Nedialkov, Y.A. & Burton, Z.F. α -amanitin blocks translocation by human RNA polymerase II. *J. Biol. Chem.* **279**, 27422–27427 (2004).
- Vassilyev, D.G. *et al.* Structural basis for substrate loading in bacterial RNA polymerase. *Nature* **448**, 163–168 (2007).
- Cramer, P. Gene transcription: extending the message. *Nature* **448**, 142–143 (2007).
- Landick, R. Active-site dynamics in RNA polymerases. *Cell* **116**, 351–353 (2004).
- Kashkina, E. *et al.* Multisubunit RNA polymerases melt only a single DNA base pair downstream of the active site. *J. Biol. Chem.* **282**, 21578–21582 (2007).
- Vassilyev, D.G., Vassilyeva, M.N., Perederina, A., Tahirov, T.H. & Artsimovitch, I. Structural basis for transcription elongation by bacterial RNA polymerase. *Nature* **448**, 157–162 (2007).
- Naji, S., Bertero, M.G., Spitalny, P., Cramer, P. & Thomm, M. Structure function analysis of the RNA polymerase cleft loops elucidates initial transcription, DNA unwinding and RNA displacement. *Nucleic Acids Res.* **36**, 676–687 (2007).
- Campbell, E.A. *et al.* Structural, functional, and genetic analysis of sorangicin inhibition of bacterial RNA polymerase. *EMBO J.* **24**, 674–682 (2005).
- Touloukhonov, I., Zhang, J., Palangat, M. & Landick, R. A central role of the RNA polymerase trigger loop in active-site rearrangement during transcriptional pausing. *Mol. Cell* **27**, 406–419 (2007).
- Sousa, R. Machinations of a Maxwellian demon. *Cell* **120**, 155–156 (2005).
- Damsma, G.E., Alt, A., Brueckner, F., Carell, T. & Cramer, P. Mechanism of transcriptional stalling at cisplatin-damaged DNA. *Nat. Struct. Mol. Biol.* **14**, 1127–1133 (2007).
- Temiakov, D. *et al.* Structural basis for substrate selection by T7 RNA polymerase. *Cell* **116**, 381–391 (2004).
- Yin, Y.W. & Steitz, T.A. The structural mechanism of translocation and helicase activity in T7 RNA polymerase. *Cell* **116**, 393–404 (2004).
- Cramer, P. Common structural features of nucleic acid polymerases. *Bioessays* **24**, 724–729 (2002).
- Abbondanzieri, E.A., Greenleaf, W.J., Shaeviz, J.W., Landick, R. & Block, S.M. Direct observation of base-pair stepping by RNA polymerase. *Nature* **438**, 460–465 (2005).
- Galbur, E.A. *et al.* Backtracking determines the force sensitivity of RNAP II in a factor-dependent manner. *Nature* **446**, 820–823 (2007).
- Chafin, D.R., Guo, H. & Price, D.H. Actions of α -amanitin during pyrophosphorylation and elongation by RNA polymerase II. *J. Biol. Chem.* **270**, 19114–19119 (1995).
- Rudd, M.D. & Luse, D.S. Amanitin greatly reduces the rate of transcription by RNA polymerase II ternary complexes but fails to inhibit some transcript cleavage modes. *J. Biol. Chem.* **271**, 21549–21558 (1996).
- Wienland, T. & Faulstich, H. Fifty years of amanitin. *Experientia* **47**, 1186–1193 (1991).
- Zanotti, G., Petersen, G. & Wienland, T. Structure-toxicity relationships in the amatoxin series. *Int. J. Pept. Protein Res.* **40**, 551–558 (1992).
- Armache, K.-J., Kettenberger, H. & Cramer, P. Architecture of the initiation-competent 12-subunit RNA polymerase II. *Proc. Natl. Acad. Sci. USA* **100**, 6964–6968 (2003).
- Brueckner, F., Hennecke, U., Carell, T. & Cramer, P. CPD damage recognition by transcribing RNA polymerase II. *Science* **315**, 859–862 (2007).
- Broennimann, E.F. *et al.* The PILATUS 1M detector. *J. Synchrotron Radiat.* **13**, 120–130 (2006).
- Kabsch, W. Automatic processing of rotation diffraction data from crystals of initially unknown symmetry and cell constants. *J. Appl. Crystallogr.* **26**, 795–800 (1993).
- McCoy, A.J., Grosse-Kunstleve, R.W., Storoni, L.C. & Read, R.J. Likelihood-enhanced fast translation functions. *Acta Crystallogr. D Biol. Crystallogr.* **61**, 458–464 (2005).
- Brunger, A.T. Version 1.2 of the Crystallography and NMR system. *Nat. Protocols* **2**, 2728–2733 (2007).
- Emsley, P. & Cowtan, K. Coot: model-building tools for molecular graphics. *Acta Crystallogr. D Biol. Crystallogr.* **60**, 2126–2132 (2004).
- Jones, T.A., Zou, J.Y., Cowan, S.W. & Kjeldgaard, M. Improved methods for building protein models in electron density maps and the location of errors in these models. *Acta Crystallogr. A* **47**, 110–119 (1991).
- Gerber, P.R. & Muller, K. MAB, a generally applicable molecular force field for structure modelling in medicinal chemistry. *J. Comput. Aided Mol. Des.* **9**, 251–268 (1995).
- Armache, K.-J., Mitterweger, S., Meinhardt, A. & Cramer, P. Structures of complete RNA polymerase II and its subcomplex Rpb4/7. *J. Biol. Chem.* **280**, 7131–7134 (2005).
- Laskowski, R.A., MacArthur, M.W., Moss, D.S. & Thornton, J.M. PROCHECK: a program to check the stereochemical quality of protein structures. *J. Appl. Crystallogr.* **26**, 283–291 (1993).